

Published in final edited form as:

Biochemistry. 2010 April 27; 49(16): 3427–3435. doi:10.1021/bi902117w.

Probing Adenine Rings and Backbone Linkages Using Base Specific Isotope-Edited Raman Spectroscopy: Application to Group II Intron Ribozyme Domain V[†]

Yuanyuan Chen[‡], Nadukkudy V. Eldho[§], T. Kwaku Dayie[§], and Paul R. Carey[‡]

T. Kwaku Dayie: dayie@umd.edu; Paul R. Carey: prc5@case.edu

[‡] Department of Biochemistry, School of Medicine, Case Western Reserve University, 10900 Euclid Avenue, Cleveland, OH 44106-4935, Tel: 216- 368-0031, Fax: 216-368-3419

[§] Departments of Chemistry and Biochemistry, College of Chemical and Life Sciences, University of Maryland, College Park, MD 20742-3360, Tel: 301-405-3165, Fax: 301-314-0386

Abstract

Raman difference spectroscopy is used to probe the properties of a 36-nt RNA molecule, “D5”, which lies at the heart of the catalytic apparatus in group II introns. For D5 that has all its adenine residues labeled with ¹³C and ¹⁵N, and utilizing Raman difference spectroscopy, we identify the conformational sensitive -C-O-P-O-C- stretching modes of the unlabeled bonds adjacent to adenine bases, as well as the adenine ring modes themselves. The phosphodiester modes can be assigned to individual adenine residues based on earlier NMR data. The effect of Mg²⁺ binding was explored by analyzing the Raman difference spectra for [D5 + Mg²⁺] minus [D5 no Mg²⁺], for D5 unlabeled, or D5 labeled with ¹³C/¹⁵N-enriched adenine. In both sets of data we assign differential features to G ring modes perturbed by Mg²⁺ binding at the N7 position. In the A labeled spectra we attribute a Raman differential near 1450 cm⁻¹ and changes of intensity at 1296 cm⁻¹ to Mg binding at the N7 position of adenine bases. The A and G bases involved in Mg²⁺ binding again can be identified using earlier NMR results. For the unlabeled D5, a change in the C-O-P-O-C stretch profile at 811 cm⁻¹ upon magnesium binding is due to a “tightening up” (in the sense of a more rigid molecule with less dynamic interchange among competing ribose conformers) of the D5 structure. For adenine labeled D5, small changes in the adenine backbone bond signatures in the 810 – 830 cm⁻¹ region suggest small conformational changes occur in the tetraloop and bulge regions upon binding of Mg²⁺. The PO₂⁻ stretching vibration, near 1100 cm⁻¹, from the non-bridging phosphate groups, probes the effect of Mg²⁺-hydrate inner-sphere interactions that cause an up-shift. In turn, the up-shift is modulated by the presence of monovalent cations since in the presence of Na⁺ and Li⁺ the up-shift is (23±2 cm⁻¹) while in the presence of K⁺ and Cs⁺ it is (13±3 cm⁻¹), a finding that correlates with the differences in hydration radii. These subtle differences in electrostatic interactions may be related to observed variations in catalytic activity. For a reconstructed ribozyme comprising domains 1–3 (D123) connected *in cis* plus domain 5 (D5) supplied in trans, cleavage of spliced exon substrates in the presence of magnesium and K⁺ or Cs⁺ is more efficient than that in the presence of magnesium with Na⁺ or Li⁺.

[†]This research was supported by the NIH GM 081420 to P.R.C and Nano-Biotechnology Award and the National Institutes of Health grant GM077326 to T.K.D.

Correspondence to: T. Kwaku Dayie, dayie@umd.edu; Paul R. Carey, prc5@case.edu.

SUPPLEMENTAL MATERIAL AVAILABLE: Calculated and experimental Raman features of unlabeled and ¹³C, ¹⁵N labeled guanosine (or GTP), cytidine (or CTP) and uridine (or UTP) are listed in Table S1. This material is available free of charge via the Internet at <http://pubs.acs.org>.

Increasingly, RNA molecules are viewed as key informational, structural, catalytic, and gene-regulatory molecules (1–3): ribosomal RNAs catalyze and regulate protein synthesis (4,5); small nuclear RNAs in combination with proteins catalyze and regulate pre-mRNA splicing (6); small nucleolar RNAs (snoRNAs) form complexes with proteins to remodel the pre-ribosomal RNAs through methylation and pseudouridylation (7); riboswitches regulate transcription or translation by directly sensing metabolites (8–11). In parallel, there is growing interest to characterize their structure, dynamics, and function using complementary biophysical tools such as NMR (12–14) and Raman spectroscopies (15–18). For RNA structural analysis, Raman spectroscopy offers some unique advantages over, and is complementary to, the two principal biophysical techniques, NMR spectroscopy and X-ray crystallography. For example, due to the intrinsic sub-picosecond time scale of the Raman effect, protonation and deprotonation events can be followed without complications from line broadening (18). While applications of Raman spectroscopy to nucleic acids began in the late 1960s and significant progress in the study of synthetic and native nucleic acids continues to be made (15,19), until now no studies have been carried out on RNA using base specific isotopic labeling to resolve spectral crowding. Using materials that were synthesized originally for NMR studies (20,21), we demonstrate the powerful potential of base specific isotopic labeling for RNA Raman difference spectroscopy. We show, as an example, that adenine (A) ring modes, as well as the RNA backbone conformations associated with A bases, can be easily distinguished from those associated with other bases. The method is easily expanded to uracil (U), cytosine (C) and guanine (G) base sets (or all base labeled RNA) to provide a general method to probe the possible mechanism and catalytic activity of RNA molecules. The approach is illustrated by incorporating isotopically labeled A bases into a highly conserved 36 nucleotide RNA domain 5 (D5) structure (Figure 1) that forms an integral part of the catalytic center of the group II intron ribozyme (1,3,20–32).

Because of the centrality of D5 to catalysis, recent high-resolution structural work has focused on isolated domains of D5 as well as structure of the complete intron without domain 6 (20, 21,24,29,31,32). Briefly, D5 adopts a lower helical stem and an upper helical stem of eight and five base pairs, respectively, separated by an internal loop. Nucleotides G10-U14 and G19-C23 form the A-form upper stem, while those from G1 to G8 and C27 to C34 form an A-form lower stem. The upper helical stem is terminated by a conserved GNRA-type (N is any nucleotide, R is a G or A) tetraloop, and a catalytic triad is positioned in the lower helix (Figure. 1). As anticipated from previous biochemical work, all structures have similar overall 3D folds with significant difference in the critical bulge region. Domain V also has two structural elements that have long been implicated in the catalytic activity of the ribozyme (22,33–36): a highly conserved sequence, AGC and an asymmetrical bulge located toward the center of domain V. The recent X-ray structure indicates two residues within the highly conserved junction region between domains 2 and 3 (J2/3) stack underneath the bulge and form a base triple directly with the three nucleotides of the triad in domain V and help to position one bulge and two triad residues to form inner sphere contacts with the critical Mg^{2+} ions via non-bridging oxygens. Our NMR titration data had predicted specific magnesium ions binding to all three sites of tetraloop, bulge, and AGC triad (21), and the recent X-ray structure has borne out the previous results (3). Importantly, the two likely catalytic metal ions identified as M1 and M2 are separated by 3.9 Å and positioned by the bulge and triad non-bridging phosphoryl oxygens (31). In addition, a monovalent K^+ ion is strategically positioned within the bulge region, underscoring the importance of monovalent ions in stabilizing the three-dimensional fold. Thus, this structure appears to fully validate the idea that domain V is the catalytic metal binding platform for the group II introns and that it likely serves to present these ions to both the 5'- and 3'-splice sites for chemistry.

In the present study, we show that RNAs prepared enzymatically give very high quality Raman spectra that are free from interfering background signals, and a minimal volume of 5 μl is

sufficient to collect solution data at millimolar concentrations. In addition to the advantages of base-specific isotopic substitution, we demonstrate that ribozyme selectivity of K^+ over Na^+ ions with functional consequence may be related to subtle differences in the interaction between Mg-hydrate and D5's PO_2^- groups, and this subtle interaction is mono-cation dependent and gives rise to different up-shifts in the PO_2^- 's stretching vibration.

MATERIALS AND METHODS

The D5 RNA sample preparation

The sample preparation was undertaken as described in Dayie (37) and Seetharaman et al. (21). Briefly, adenine base-specific $^{13}C/^{15}N$ labeled RNA samples were synthesized by *in vitro* transcription with T7 RNA polymerase from synthetic DNA templates (Operon Technologies, Inc, Alameda, CA) using isotopically labeled ATPs (Isotec, OH) (21,37). The T7 RNA polymerase was overexpressed in *Escherichia coli* BL21 (DE3) and purified on a Ni-chelating sepharose column (Pharmacia). The DNA promoter sequence has the sequence: 5' CTA ATA CGA CTC ACT ATA G-3'. The corresponding template strand, or bottom strand, used for NMR and Raman analyses was 5'-g AAC CGT ACG TGC GAC TTT CAT CGC ATA CGG CTC c TAT AGT GAG TCG TAT TAG-3' (lower case letters represent non-native nucleotides introduced to improve transcription yield). The optimal transcription conditions were 15 mM total NTP and 13.7 mM Mg^{2+} in a transcription buffer of 40 mM Tris-HCl, pH 8.1, 1 mM spermidine, 5 mM dithiothreitol (DTT), 0.01% Triton X-100, 80 mg/ml PEG 8000, 300 nM each DNA strand, and 1.5 μ l T7 polymerase (optimized amount) per 40 μ l of transcription volume. After three hours of incubation at 310 K, the transcription reaction was extracted with phenol/chloroform/isoamyl alcohol (25:24:1) to remove the T7 RNA polymerase. The crude RNA was purified using denaturing preparative gel electrophoresis (37). The lyophilized D5 RNA stocks were resuspended in water and dialyzed in a Biodialyzer (Nestgroup, Cambridge, MA) with a 500 MWCO membrane (Nestgroup, Cambridge, MA) for 24 hours each against 0.5 M potassium chloride, 10 mM EDTA, and then 0.1 mM EDTA, and finally against two changes of ddH₂O water. After dialysis, the RNA was lyophilized and resuspended into each specific buffer to a final concentration of 2 mM in 40 mM MOPS buffer (pH 7.5) supplemented with the following salts: a) 100 mM KCl; b) 100 mM NaCl; c) 100 mM KCl and 25 mM $MgCl_2 \cdot 6H_2O$; d) 100 mM NaCl and 25mM $MgCl_2 \cdot 6H_2O$.

Raman spectroscopy

Raman spectra were collected using a Raman microscope with 5 μ L hanging drops of RNA samples (38). A drop of sample is placed on a cover slide which is sealed on top of a well of crystallization tray with buffer on the bottom. The 647.1 nm (150 mW) laser beam was focused in the drop by viewing through a video camera mounted on the microscope. The back scattered light from the focused volume of sample was collected through the microscope and processed through a spectrograph and a charge coupled detector (CCD). Each Raman spectrum was acquired for 100 seconds. A "pure" D5 spectrum was obtained from a subtraction of [D5 in buffer] minus [corresponding buffer], normalized by an intense buffer peak at 1045 cm^{-1} . Then, to compare different D5 samples, a secondary subtraction [A-labeled D5] minus [unlabeled D5] was carried out, using the non-bridging phosphate peak near 1100 cm^{-1} for normalization. Other Raman difference spectra mentioned in the text were obtained using the same subtraction method.

Calculations

Ab initio quantum mechanical calculations were performed to predict the vibrational modes and Raman spectra of adenosine (Table 1), guanosine, uridine and cytidine (Supplemental Material Table S1) using Gaussian 03 (39). Calculations were set at the DFT level using the 6-31+G(d) basis set. DFT calculations were carried out with Becke's three-parameter hybrid

method using the correlation functional of Lee, Yang, and Parr (B3LYP), with 20% HF exact exchange mixing. A standard scaling factor of 0.961 was applied to the calculated values.

D1235 RNA preparation

To carry out the functional assay, it was necessary to redesign the group II intron ribozyme into a two part RNA enzyme: one piece is made up of domains 1, 2, 3, and 5 (D1235) that contains all the catalytic machinery; a second piece is made up of ligated exon 1 and exon 2 fragments (E1E2). The D1235 RNA is transcribed by *in vitro* transcription by using a mutant T7 RNA Polymerase, unlabeled NTPs and a PCR generated DNA template, using established protocols (40). The His-tag mutant T7 RNA Polymerase is overexpressed in *E. coli* BL21 (DE3) and purified on a Ni-chelating Sepharose column (41,42). An RNA containing intron domain 1–3 and 5 is transcribed from PCR generated DNA as follows. D1235 is amplified from the original D123 (20,43) construct with an upstream T7 RNA polymerase promoter sequence (5'-GAA TTC TAA TAC GAC TCA CTA TAGG3') and a downstream primer which contains the 35 nucleotides of domain 5 (5'-GAA CCG TGC TTG CGA CTT TCA TCG CAC ACG GCT CCC ATT TAA TAA GTC TGC AGC C3') and 20 nucleotides from the 3' end of domain 3. The resultant PCR product was agarose gel purified, cloned into a TA vector (Invitrogen) and transformed into chemically competent *E. Coli* cells (Invitrogen). A plasmid from a single colony (ampicillin-resistant) was isolated and sequence verified. This plasmid was subsequently used for all the preparation of D1235 RNA used in the functional assays.

For transcription of D1235 RNA, the DNA template was generated by PCR amplification of a fragment containing an upstream T3 priming site and the complete D5 sequence and 20 nucleotides from the 3' end of domain 3. The D1235 RNA was made by *in vitro* transcription in a reaction containing Transcription buffer (40 mM Tris-HCl (pH 8.0), 1 mM spermidine, 0.01% (v/v) Triton X-100 and 10 mM DTT), 0.2 ug of mutant T7 RNA polymerase, 0.2 U of RNase Inhibitor (Ambion and/or New England Biolabs), 0.2 U of inorganic pyrophosphatase (New England Biolabs), 1 ug of PCR generated DNA template, 18 mM MgCl₂·6H₂O and 10 mM each NTP. The reaction was incubated for 4 hours at 37°C. After 4 hours, 0.2 U of Turbo DNase (Ambion) was added and incubated for another 15 minutes. The reaction mixture was purified by anion exchange chromatography without phenol-chloroform extraction. Anion-exchange chromatography was used to separate the unincorporated nucleotides and proteins from the transcribed RNA, and a 8% PAGE/8M Urea/1xTBE gel was used to verify the purity of the RNA construct.

Spliced exon reopening reaction (SER reaction)

The group II intron from *Pylaiella littoralis* (PL) can support splicing at low magnesium ion concentrations (20,43,44) unlike the group II intron from Ai5γ, which requires high salt conditions (100 mM MgCl₂, 500 mM ammonium sulfate or 1 M KCl) (45). The difference Raman spectrum of domain 5 (D5) hairpin RNA in the presence of various monovalent and magnesium ions showed a difference in Raman shift of the vibrational mode of the phosphate backbone in D5. We wondered if this difference in Raman shift could be correlated with the splicing efficiency of E1E2 substrate supplied in *trans* with D1235 RNA. To test this hypothesis, we used a splicing reaction buffer of 40 mM MOPS (X⁺) (pH 7.50) and 10 mM MgCl₂ containing 100 mM XCl, where X = Li⁺, Na⁺, K⁺ and Cs⁺. To visualize the cleaved fluorescently labeled substrate (Alexa647-E1E2), we used a previously developed fluorescence in-gel method (20,44). To ensure there are no competing monovalent ions, we dialyzed D1235 extensively against water for 24 hours and then against MOPS (X⁺) (pH7.50) for 12 hours.

The D1235 RNA (0.5 μM) and Alexa647-E1E2 (37.5 nM) were individually mixed with 40 mM MOPS(X⁺) and 100 mM XCl and heated to 90 °C for one minute and pre-folded at 42°C for 2 hours. The cleavage reaction was initiated by adding 10 mM magnesium chloride to the

pre-folded binary complex of D12335 and E1E2. At each time point (0, 30, 60, 120, 180 minutes), 5 μ l aliquot of the reaction is quenched using the stopping buffer (100 mM EDTA pH 8.0, 10% glycerol). The extent of the cleavage was visualized on a Molecular Imager (Storm imager, Molecular dynamics), and the uncleaved and cleaved substrate intensities were quantified using Image Quant (20,44).

RESULTS AND DISCUSSION

D5 labeled with adenine bases containing ^{15}N and ^{13}C at all nitrogen and carbon sites

Raman difference spectroscopy is used to identify the adenine (A) ring and A-flanking phosphodiester backbone modes in D5 RNA, by subtracting the spectra of unlabeled and fully-A-labeled (with all ^{15}N and ^{13}C atoms) samples. By the help of a Raman microscope, spectra were recorded for both samples in 5 microliter hanging drops. By subtracting the D5-unlabeled from the D5-A-labeled spectrum, the adenine ring modes, which are normally obscured by guanine ring modes in RNA Raman spectra, could be unambiguously identified. For example, the negative peak at 1575 cm^{-1} in Figure 2C is due to an A ring mode from unlabeled As, while the corresponding A labeled mode appears as a positive feature at 1520 cm^{-1} . Thus, the adenine ring modes seen in Figure 2C at 1575 , 1508 , 1481 , 1377 , and 1338 cm^{-1} are clearly detected, although they are obscured by other base (primarily G) modes in the unlabeled spectrum (Figure 2A).

The peak positions identified above correlate strongly with adenine ring modes in unlabeled and isotopic labeled ATP, which undergo very similar Raman shifts upon ^{13}C and ^{15}N enrichment (Figure 3, Table 1). Thus, the assignments in Table 1 given for the adenine-ring modes can be transferred to RNA assignments. It is notable that the symmetric stretching motions of the PO_2^- groups near 1100 cm^{-1} , in Figure 2A and 2B, subtract essentially to zero in the difference spectrum, in Figure 2C. The PO_2^- group is essentially an “independent oscillator”, in the sense that it does not couple extensively to the motions of C3' and C5' ribose atoms. Strategies, identical to that for adenine, can be used to isolate C, G and U ring modes. This facile identification of all four ring modes (adenine, cytosine, guanine, and uracil) has implications for probing chemical events involving bases in RNA catalysis (18,46–48). This is particularly useful when, as in the present case, the labeled base occurs mostly in sites of biological relevance.

A further important outcome of the difference Raman data seen in Figure 2C is the spectral region of $800 - 850\text{ cm}^{-1}$, that has contributions from D5's phosphodiester backbone. It is known that stretching motions of the $-\text{C}-\text{O}-\text{P}-\text{O}-\text{C}-$ bonds are very dependent on conformation (49). Thus, the peak at 812 cm^{-1} in Figure 2A is a signature of all the phosphodiester bonds of the backbone in the classical A-form RNA, where the ribose pucker is C3'-endo. In the difference spectrum in Figure 2C (A-labeled minus unlabeled) the “negative” features at 827 and 815 cm^{-1} are from unlabeled phosphodiester bonds that are linked to either the C3' or C5' or both C3' and C5' carbons of labeled adenine. These vibrational modes due to the corresponding bonds $-\text{C}-\text{O}-\text{P}-\text{O}-\text{C}-$ labeled at C3' or C5' or both C3' and C5' carbons are downshifted in the spectrum of labeled D5 (although this detail cannot be seen in the trace, Figure 2B) and thus in Figure 2C features due to the unlabeled bonds appear in the difference spectrum in the “negative sense”, and features due to labeled bonds appear in the difference spectrum in the “positive sense”. Figure 4 shows a “zoomed in” version of the 800 cm^{-1} region and compares the effect of adding Mg^{2+} , the latter will be discussed below. When interpreting the data in Figure 4 it is essential to remember that the time scale of Raman spectroscopy is sub-picosecond. The adenines in the loop and bulge regions possess considerable conformational flexibility, and the Raman spectra of the adjacent phosphodiester bonds, whose modes are seen in Figure 4 (in the “negative” direction) reflect an instantaneous snapshot of all the (probably interchanging) conformers present. The NMR experiments by Seetharaman

et al.(21) show that A16 (loop), A24 and A 25 (bulge) are mostly in the C2'-endo sugar pucker. These make major contributions to the “negative” intensity at 826 cm^{-1} as shown in Figure 4. Adenine conformational units that spend a significant portion of their time in A-space (with the ribose C3'-endo) contribute to the intensity at 813 cm^{-1} . Another means of analyzing the data is to compare the spectra in the 800 cm^{-1} region shown in Figure 5. These profiles are unlabeled D5 minus buffer and A- labeled D5 minus buffer, and the profiles have been fitted using the minimum number of Gaussian components. The feature at 824 cm^{-1} (purple) in Figure 5A (unlabeled D5 minus buffer) is missing in the A labeled-D5 profile, indicating that this frequency is from A16, A24 and A25 bases. Thus the modes detected from unlabeled A-linkages provide a means to follow changes in backbone conformation in the tetraloop and bulge regions of RNA.

The effects of binding of magnesium hydrate to D5

The Raman difference spectrum of [unlabeled D5 + 25 mM Mg^{2+}] minus [unlabeled D5 with no Mg^{2+}] is shown in Figure 6A. The intense differential features near 1489/1479 and 1329/1320 cm^{-1} are dominated by guanine ring modes. The differential feature near 1489/1479 cm^{-1} has been assigned to a guanine ring mode that is perturbed by binding of magnesium hydrate at N7 (50). The NMR titration of D5 with magnesium hydrate (21) showed chemical shift changes at N7 of G15 and G19. Thus, it is likely that major contributors to the 1489/1479 differential are G residues G15 and G19 in the tetraloop region. The NMR results also indicate that G8, G12, G30 and G31 likely bind Mg^{2+} at their N7 positions. It is noteworthy that the mode seen near 1485 cm^{-1} , seen in the UVR spectrum of G residues, is sensitive to H-bonding at N7 (51). The differential at 1329/1320 in Figure 6A is also assigned to a G ring mode, based on the spectroscopic data in Supplemental Material Table S1, this too is ascribed to Mg^{2+} binding at N7 in the bases listed above, and this is the first time the differential at 1325 cm^{-1} has been noted. The differential at 785/765 cm^{-1} is assigned to the effect of Mg^{2+} on C and/or U base ring modes (Supplemental Table S1). The NMR titration data (21) suggest U9, U20 and C29 as possible sites of interaction, but the mode of magnesium hydrate interaction with cytosine and uracil is not well characterized. However, the recent x-ray structure of the group II intron from the gram-positive bacterium *Oceanobacillus iheyensis* indicates that magnesium and potassium ions chelate some of these bases (3).

Some insight into the effect of magnesium hydrate on adenine ring modes can be obtained from the difference spectrum in Figure 6B, [A-labeled D5 with 10 mM Mg^{2+}] minus [A-labeled D5 no Mg^{2+}]. In Figure 6B the effect of Mg^{2+} on the ring modes from G near 1490/1479 cm^{-1} and 1328/1320 cm^{-1} duplicate the “differentials” seen in Figure 6A for unlabeled material. This confirms the assignment of G-ring... Mg^{2+} interaction (50). However, a small but reproducible additional differential at 1454/1447 cm^{-1} is assigned to Mg^{2+} making inner-sphere contact at the N7 position of adenine rings; this is based on the presence of the adenine ring mode seen in Figure 3 at 1447 cm^{-1} in ^{13}C and ^{15}N labeled ATP. In D5 specific isotopic substitution in the A rings shifts the A mode to a spectral window where the differential can be observed. We also suggest that the negative feature seen in Figure 6B at 1296 cm^{-1} is due to Mg^{2+} causing a change in the intensity of the adenine ring mode seen at this position in Figure 3B for labeled ATP. Again, the NMR titrations (ref. 21, Figure 7) identify A24 (bulge region), A17 (tetraloop) and A2 (catalytic triad) as likely candidates causing the above Raman changes.

Another notable feature in Figure 6A (Raman difference spectrum of unlabeled [D5 with 25 mM Mg^{2+}] minus [D5 with no Mg^{2+}]) is the increase in intensity at 811 cm^{-1} in the presence of 25 mM Mg^{2+} . This is due to the fact that the population of ribose conformations in the classic A-form (3'-endo) increases slightly as Mg^{2+} binds. This is a small effect since the increase seen in Figure 6A is about 6% ($\pm 1\%$) of the height of the parent peak (ie the peak prior to

subtraction in [D5 with no Mg^{2+}]). The increase in height is accompanied by a decrease in width at half height from $16.2 (\pm 0.2)$ to $15.2 (\pm 0.2) \text{ cm}^{-1}$. This may represent a small change in the populations that are in dynamic equilibrium in the flexible tetraloop and bulge regions spread over several residues. More insight is gained from analyzing the conformations of the $-\text{C}-\text{O}-\text{P}-\text{O}-\text{C}-$ bonds next to the adenine-bases that constitute the “negative” profile seen in the $800 - 850 \text{ cm}^{-1}$ range in Figure 4. This figure demonstrates that the addition of 10 mM Mg^{2+} brings about a slight but reproducible increase in the shoulder 826 cm^{-1} . A similar increase of about $4\% (\pm 1\%)$ is seen for the 824 cm^{-1} component in Figure 5A in the presence of Mg^{2+} (data not shown). These data taken together show that there is likely a small increase in 2'-endo conformations next to A residues in the presence of 10 mM Mg^{2+} . Detecting this small overall change (Figures 4 and 5) in conformational equilibria is a novel insight from Raman spectroscopy with its sub-picosecond intrinsic time scale.

Mg^{2+} binding at PO_2^- groups in the presence of monovalent cations

Recently, we presented evidence that Mg^{2+} penta or tetra hydrate binds inner-sphere to several PO_2^- groups of the RNA molecule HDV (hepatitis delta virus) in single crystals and causes the PO_2^- symmetric stretch to shift from 1100 to 1117 cm^{-1} (52). In addition, we have gathered a plethora of additional data on a wide variety of RNA molecules (unpublished work) that show a 20 to 25 cm^{-1} up-shift in the PO_2^- stretch caused by Mg^{2+} binding in the presence of Na^+ . In this sense the effect of Mg^{2+} binding to the PO_2^- groups of D5 initially appeared to be atypical, since the differential in the difference spectrum for 25 mM Mg^{2+} binding to 3 mM D5 in the presence of 100 mM KCl occurs at 1103 and 1092 cm^{-1} (Figure 7A). This 11 cm^{-1} upshift represents the smallest yet seen for Mg^{2+} hydrate binding to PO_2^- groups. Further experimentation revealed that this up-shift increases to 20 cm^{-1} in the presence of 20 mM Mg^{2+} 100 mM NaCl , with no KCl present (Figure 7B). Moreover, in the K^+ background, the PO_2^- peak at 1103 moves to 1111 cm^{-1} in the presence of 40 mM Mg^{2+} (data not shown). The detailed geometry of Mg^{2+} hydrate at PO_2^- sites and its relationship to the frequency up-shift is very subtle and is not fully understood (52). However, these results indicate that the inner sphere interaction between the negatively charged PO_2^- groups and Mg^{2+} (probably as the pentahydrate) is modulated by the presence of mono cations. Moreover, this modulation can be minimized at high concentrations of magnesium via increasing competition at the anion.

In order to explore these effects further we measured the effect on the $\text{PO}_2^- \dots \text{Mg}^{2+}$ interaction in monocation backgrounds throughout the Group I series Li^+ , Na^+ , K^+ or Cs^+ . The data in Table 2 show that at 100 mM levels of monocation and 20 mM of Mg^{2+} , there is a tendency for the shift in the PO_2^- symmetric stretch to decrease as the hydrated radius of the monocation increases. In the absence of magnesium the PO_2^- vibrations are identical within experimental error for each of the four monovalent ions with an average value of $1093 \pm 1 \text{ cm}^{-1}$. Since the competition between the monocations and hydrated magnesium for the PO_2^- sites likely involves hydrated monocations it is important to observe that there is a clear delineation between the small hydrated radii of Li^+ and Na^+ (2.1 \AA and 2.45 \AA , respectively) and the larger values for K^+ and Cs^+ (2.75 \AA and 3.1 \AA , respectively). We hypothesize that the larger hydrated cations are most effective in reducing the magnesium hydrate PO_2^- interaction and thus reducing the up-shift in PO_2^- symmetric stretch in the presence of magnesium.

Intriguingly this selective monovalent ion effect correlates with catalytic activity of the group II Intron ribozyme (Figure 8). Previous studies indicated the first two introns (1 and 2) of the mitochondrial genes encoding the large subunit (LSU) of the ribosomal RNA from brown algae are more reactive under elevated concentrations of NH_4^+ and K^+ monovalent cations (43), which is also the case for other group II self-splicers (43,53,54). But unlike previous group II intron self-splicers, the second LSU (LSU/2) intron self-splices at unusually low Mg^{2+} ions (43). We tested the hypothesis that in the presence of monovalent cations Mg^{2+} hydrate will

cleave an RNA substrate in proportion to the hydrated radius of the monovalent ion. Of the six domains of group II introns, domains 1 through 3 (D123) and domain 5 (D5) are necessary and sufficient to cleave the bond joining the 5'-exon (E1) and the 3'-exon (E2) in the reverse of the second step of splicing (20,44,54), termed the spliced exon reopening reaction (SER). We use this SER reaction for the in-gel fluorescent assay (44) to monitor the cleavage of a 37.5 nM substrate E1E2 labeled with alexa 647 fluor (A647-E1E2 substrate) in the presence of 10 mM Mg^{2+} and 100 mM of XCl (where X= Li^+ , Na^+ , K^+ , and Cs^+) and saturating amount of D1235 (0.5 μ M) (Figure 8). The extent of the cleavage reaction was monitored by calculating either the amount of product or substrate at each time point (0, 30, 60, 120, and 180 minutes). As can be seen in Figure 8, in the presence of 100 mM LiCl or NaCl, magnesium ions are substantially handicapped (<20% efficient) in potentiating cleavage of substrate, whereas in the presence of KCl or CsCl magnesium ions efficiently (~80%) potentiate substrate cleavage. These efficient cleavages anti-correlate with the change in Raman shift (Figure 9) and importantly shows a strong dependence on the hydrated radii, with the larger hydrated cations more effective in accelerating cleavage by magnesium.

This monovalent ion selectivity has been observed in other RNAs in the past. It has been known for close to 40 years that the activities of both subunits of the ribosome depend on K^+ and NH_4^+ , and these are reversibly inhibited by Na^+ or other alkali metals ions (55,56). Similarly, the splicing activity of a small *Azoarcus* group I intron is stimulated several fold by K^+ , but not by Li^+ , Na^+ , or in this case, Cs^+ ions (57).

CONCLUSION

The results of the present study emphasize the power of combining Raman analysis of small RNA molecules with NMR studies where both techniques utilize samples labeled with ^{13}C and ^{15}N at one class of base, illustrated in the present case by labeling all adenine bases in D5. The advantages for Raman are two fold. Labeling moves A ring modes into spectral regions where they can be identified and analyzed without interference from the usually overlapping G modes. Moreover, the NMR identification of individual A rings perturbed by Mg^{2+} binding, for example, allows us to assign changes in A modes in the Raman spectra to these individual bases. In addition, the base specific labeling allows us to identify modes from the phosphodiester backbone and we can probe the conformation of just the bonds flanking A bases. Again, the results from the NMR experiments allow us to identify which A bases are involved in conformational events. There are further experimental outcomes from our approach. Our samples are produced *in vitro* enzymatically and this had the unexpected advantage of providing very high quality materials that furnish exemplary Raman data (in contrast, RNA samples examined by us that have been produced by chemical synthesis are often difficult to produce in a clean luminescence-free format. This may have the unfortunate consequence of hindering attempts at inserting labeled bases at a single targeted position, since the chemically labeled construct may be irredeemably luminescent). Furthermore, we have shown that only 5 microliters of sample are needed and this bodes well for future studies on relatively small amounts of RNA. Finally, based on the present data we postulate that Mg^{2+} hydrate binds to phosphate in the presence of K^+ slightly differently than in the presence of Na^+ , and importantly this binding correlates with catalytic activity of the group II Intron ribozyme from brown algae; this monovalent ion selectivity has been observed in other RNAs in the past (55,56) suggesting that those RNA elements may also exhibit Raman signatures for the PO_2^- stretch similar to those described here.

Supplementary Material

Refer to Web version on PubMed Central for supplementary material.

Acknowledgments

PRC and YC acknowledge support from CWRU's computer facility, and TKD for valuable discussions with Andrei Vedernikov.

List of Abbreviations/key words

D5	domain V of group II intron
D123	domain I, II and III of group II intron
D1235	domain I, II, III and V of group II intron
snoRNA	small nucleolar RNA
MWCO	molecular weight cut-off
EDTA	ethylenediaminetetraacetic acid
MOPS	3-(N-morpholino)propanesulfonic acid
ddH ₂ O	double-distilled water
CCD	charge coupled device
DFT	density function theory
HF	Hartree–Fock method
FPLC	fast protein liquid chromatography
PAGE	polyacrylamide gel electrophoresis
TBE	tris-borate-EDTA buffer for gel electrophoresis separation of RNA or DNA
SER reaction	spliced exon reopening reaction
ATP	Adenosine-5'-triphosphate
LSU	large subunit of ribosomal RNA
E1	the 5' exon
E2	the 3' exon

References

1. Pyle, AM.; Lambowitz, AM. The RNA World. Gesteland, RF.; Cech, TR.; Atkins, JF., editors. Cold Spring Harbor Lab Press; Cold Spring Harbor, NY: 2006. p. 469-505.
2. Cech TR. The generality of self-splicing RNA: relationship to nuclear mRNA splicing. *Cell* 1986;44:207–210. [PubMed: 2417724]
3. Toor N, Keating KS, Taylor SD, Pyle AM. Crystal structure of a self-spliced group II intron. *Science* 2008;320:77–82. [PubMed: 18388288]
4. Korostelev A, Ermolenko DN, Noller HF. Structural dynamics of the ribosome. *Curr Opin Chem Biol* 2008;12:674–683. [PubMed: 18848900]
5. Steitz TA. A structural understanding of the dynamic ribosome machine. *Nat Rev Mol Cell Biol* 2008;9:242–253. [PubMed: 18292779]
6. Wahl MC, Will CL, Luhrmann R. The spliceosome: design principles of a dynamic RNP machine. *Cell* 2009;136:701–718. [PubMed: 19239890]
7. Boisvert FM, van Koningsbruggen S, Navascues J, Lamond AI. The multifunctional nucleolus. *Nat Rev Mol Cell Biol* 2007;8:574–585. [PubMed: 17519961]
8. Breaker RR. Riboswitches: from ancient gene-control systems to modern drug targets. *Future Microbiol* 2009;4:771–773. [PubMed: 19722830]

9. Loh E, Dussurget O, Gripenland J, Vaitkevicius K, Tiensuu T, Mandin P, Repoila F, Buchrieser C, Cossart P, Johansson J. A trans-acting riboswitch controls expression of the virulence regulator PrfA in *Listeria monocytogenes*. *Cell* 2009;139:770–779. [PubMed: 19914169]
10. Poiata E, Meyer MM, Ames TD, Breaker RR. A variant riboswitch aptamer class for S-adenosylmethionine common in marine bacteria. *RNA* 2009;15:2046–2056. [PubMed: 19776155]
11. Weigand JE, Suess B. Aptamers and riboswitches: perspectives in biotechnology. *Appl Microbiol Biotechnol* 2009;85:229–236. [PubMed: 19756582]
12. Akke M, Fiala R, Jiang F, Patel D, Palmer AG 3rd. Base dynamics in a UUCG tetraloop RNA hairpin characterized by ¹⁵N spin relaxation: correlations with structure and stability. *RNA* 1997;3:702–709. [PubMed: 9214654]
13. Dayie KT, Brodsky AS, Williamson JR. Base flexibility in HIV-2 TAR RNA mapped by solution (¹⁵N, (¹³C) NMR relaxation. *J Mol Biol* 2002;317:263–278. [PubMed: 11902842]
14. Eldho NV, Dayie KT. Internal bulge and tetraloop of the catalytic domain 5 of a group II intron ribozyme are flexible: implications for catalysis. *J Mol Biol* 2007;365:930–944. [PubMed: 17098254]
15. Gong B, Chen JH, Yajima R, Chen Y, Chase E, Chadalavada DM, Golden BL, Carey PR, Bevilacqua PC. Raman crystallography of RNA. *Methods* 2009;49:101–111. [PubMed: 19409996]
16. Spiro, TG. Biological applications of Raman spectroscopy. Vol. 1. 1987.
17. Tu, AT. Raman spectroscopy in biology: principles and applications. Wiley; New York: 1982.
18. Guo M, Spitale RC, Volpini R, Krucinska J, Cristalli G, Carey PR, Wedekind JE. Direct Raman measurement of an elevated base pKa in the active site of a small ribozyme in a precatalytic conformation. *J Am Chem Soc* 2009;131:12908–12909. [PubMed: 19702306]
19. Hudson SD, Chumanov G. Bioanalytical applications of SERS (surface-enhanced Raman spectroscopy). *Anal Bioanal Chem* 2009;394:679–686. [PubMed: 19343331]
20. Gumbs OH, Padgett RA, Dayie KT. Fluorescence and solution NMR study of the active site of a 160-kDa group II intron ribozyme. *RNA* 2006;12:1693–1707. [PubMed: 16894219]
21. Seetharaman M, Eldho NV, Padgett RA, Dayie KT. Structure of a self-splicing group II intron catalytic effector domain 5: parallels with spliceosomal U6 RNA. *RNA* 2006;12:235–247. [PubMed: 16428604]
22. Abramovitz DL, Friedman RA, Pyle AM. Catalytic role of 2'-hydroxyl groups within a group II intron active site. *Science* 1996;271:1410–1413. [PubMed: 8596912]
23. Boudvillain M, Pyle AM. Defining functional groups, core structural features and inter-domain tertiary contacts essential for group II intron self-splicing: a NAIM analysis. *EMBO J* 1998;17:7091–7104. [PubMed: 9843513]
24. Dayie KT, Padgett RA. A glimpse into the active site of a group II intron and maybe the spliceosome, too. *RNA* 2008;14:1697–1703. [PubMed: 18658120]
25. Fedorova O, Su LJ, Pyle AM. Group II introns: highly specific endonucleases with modular structures and diverse catalytic functions. *Methods* 2002;28:323–335. [PubMed: 12431436]
26. Pyle AM. Role of metal ions in ribozymes. *Met Ions Biol Syst* 1996;32:479–520. [PubMed: 8640529]
27. Pyle AM. Metal ions in the structure and function of RNA. *J Biol Inorg Chem* 2002;7:679–690. [PubMed: 12203005]
28. Qin PZ, Pyle AM. The architectural organization and mechanistic function of group II intron structural elements. *Curr Opin Struct Biol* 1998;8:301–308. [PubMed: 9666325]
29. Sigel RK, Sashital DG, Abramovitz DL, Palmer AG, Butcher SE, Pyle AM. Solution structure of domain 5 of a group II intron ribozyme reveals a new RNA motif. *Nat Struct Mol Biol* 2004;11:187–192. [PubMed: 14745440]
30. Sigel RK, Vaidya A, Pyle AM. Metal ion binding sites in a group II intron core. *Nat Struct Biol* 2000;7:1111–1116. [PubMed: 11101891]
31. Toor N, Rajashankar K, Keating KS, Pyle AM. Structural basis for exon recognition by a group II intron. *Nat Struct Mol Biol* 2008;15:1221–1222. [PubMed: 18953333]
32. Zhang L, Doudna JA. Structural insights into group II intron catalysis and branch-site selection. *Science* 2002;295:2084–2088. [PubMed: 11859154]

33. Chanfreau G, Jacquier A. Catalytic site components common to both splicing steps of a group II intron. *Science* 1994;266:1383–1387. [PubMed: 7973729]
34. Boulanger SC, Belcher SM, Schmidt U, Dib-Hajj SD, Schmidt T, Perlman PS. Studies of point mutants define three essential paired nucleotides in the domain 5 substructure of a group II intron. *Mol Cell Biol* 1995;15:4479–4488. [PubMed: 7623838]
35. Peebles CL, Zhang M, Perlman PS, Franzen JS. Catalytically critical nucleotide in domain 5 of a group II intron. *Proc Natl Acad Sci U S A* 1995;92:4422–4426. [PubMed: 7538669]
36. Schmidt U, Podar M, Stahl U, Perlman PS. Mutations of the two-nucleotide bulge of D5 of a group II intron block splicing in vitro and in vivo: phenotypes and suppressor mutations. *RNA* 1996;2:1161–1172. [PubMed: 8903346]
37. Dayie KT. Resolution enhanced homonuclear carbon decoupled triple resonance experiments for unambiguous RNA structural characterization. *J Biomol NMR* 2005;32:129–139. [PubMed: 16034664]
38. Carey PR. Raman crystallography and other biochemical applications of Raman microscopy. *Annu Rev Phys Chem* 2006;57:527–554. [PubMed: 16599820]
39. Frisch, A.; Frisch, MJ.; Trucks, GW. Gaussian. Inc; Wallingford, CT: 2003.
40. Milligan JF, Uhlenbeck OC. Synthesis of small RNAs using T7 RNA polymerase. *Methods Enzymol* 1989;180:51–62. [PubMed: 2482430]
41. He B, Rong M, Durbin RK, McAllister WT. A mutant T7 RNA polymerase that is defective in RNA binding and blocked in the early stages of transcription. *J Mol Biol* 1997;265:275–288. [PubMed: 9018042]
42. He B, Rong M, Lyakhov D, Gartenstein H, Diaz G, Castagna R, McAllister WT, Durbin RK. Rapid mutagenesis and purification of phage RNA polymerases. *Protein Expr Purif* 1997;9:142–151. [PubMed: 9116496]
43. Costa M, Fontaine JM, Loiseaux-de Goer S, Michel F. A group II self-splicing intron from the brown alga *Pylaiella littoralis* is active at unusually low magnesium concentrations and forms populations of molecules with a uniform conformation. *J Mol Biol* 1997;274:353–364. [PubMed: 9405145]
44. Dayie KT, Gumbs OH, Eldho NV, Seetharaman M, Thompson M. In-gel fluorescence probing of RNA-RNA interactions. *Anal Biochem* 2007;362:278–280. [PubMed: 17275775]
45. Su LJ, Brenowitz M, Pyle AM. An alternative route for the folding of large RNAs: apparent two-state folding by a group II intron ribozyme. *J Mol Biol* 2003;334:639–652. [PubMed: 14636593]
46. Reiter NJ, Blad H, Abildgaard F, Butcher SE. Dynamics in the U6 RNA intramolecular stem-loop: a base flipping conformational change. *Biochemistry* 2004;43:13739–13747. [PubMed: 15504036]
47. Venditti V, Clos L 2nd, Niccolai N, Butcher SE. Minimum-energy path for a u6 RNA conformational change involving protonation, base-pair rearrangement and base flipping. *J Mol Biol* 2009;391:894–905. [PubMed: 19591840]
48. Billingham BE, Oladepo SA, Loppnow GR. pH-dependent UV resonance Raman spectra of cytosine and uracil. *J Phys Chem B* 2009;113:7392–7397. [PubMed: 19438283]
49. Carey, PR. *Molecular Biology*. Academic Press; New York: 1982. *Biochemical Applications of Raman and Resonance Raman Spectroscopies*.
50. Chen JH, Gong B, Bevilacqua PC, Carey PR, Golden BL. A catalytic metal ion interacts with the cleavage Site G.U wobble in the HDV ribozyme. *Biochemistry* 2009;48:1498–1507. [PubMed: 19178151]
51. Mukerji I, Shiber MC, Fresco JR, Spiro TG. A UV resonance Raman study of hairpin dimer helices of d(A–G)₁₀ at neutral pH containing intercalated dA residues and alternating dG tetrads. *Nucleic Acids Res* 1996;24:5013–5020. [PubMed: 9016674]
52. Gong B, Chen Y, Christian EL, Chen JH, Chase E, Chadavada DM, Yajima R, Golden BL, Bevilacqua PC, Carey PR. Detection of inner-sphere interactions between magnesium hydrate and the phosphate backbone of the HDV ribozyme using Raman crystallography. *J Am Chem Soc* 2008;130:9670–9672. [PubMed: 18593125]
53. Hebbar SK, Belcher SM, Perlman PS. A maturase-encoding group IIA intron of yeast mitochondria self-splices in vitro. *Nucleic Acids Res* 1992;20:1747–1754. [PubMed: 1579468]
54. Jarrell KA, Peebles CL, Dietrich RC, Romiti SL, Perlman PS. Group II intron self-splicing. Alternative reaction conditions yield novel products. *J Biol Chem* 1988;263:3432–3439. [PubMed: 2830285]

55. Miskin R, Zamir A, Elson D. Inactivation and reactivation of ribosomal subunits: the peptidyl transferase activity of the 50 s subunit of Escherichia coli. *J Mol Biol* 1970;54:355–378. [PubMed: 4924204]
56. Zamir A, Miskin R, Elson D. Inactivation and reactivation of ribosomal subunits: amino acyl-transfer RNA binding activity of the 30 s subunit of Escherichia coli. *J Mol Biol* 1971;60:347–364. [PubMed: 4938735]
57. Basu S, Rambo RP, Strauss-Soukup J, Cate JH, Ferre-D'Amare AR, Strobel SA, Doudna JA. A specific monovalent metal ion integral to the AA platform of the RNA tetraloop receptor. *Nat Struct Biol* 1998;5:986–992. [PubMed: 9808044]
58. Marcus Y. Ionic radii in aqueous solutions. *Chem Rev* 1988;88:1475–1498.
59. Ohtaki H, Radnai T. Structure and dynamics of hydrated ions. *Chem Rev* 1993;93:1157–1204.
60. Joung IS, Cheatham TE III. Determination of alkali and halide monovalent ion parameters for use in explicitly solvated biomolecular simulations. *J Phys Chem B* 2008;112:9020–9041. [PubMed: 18593145]

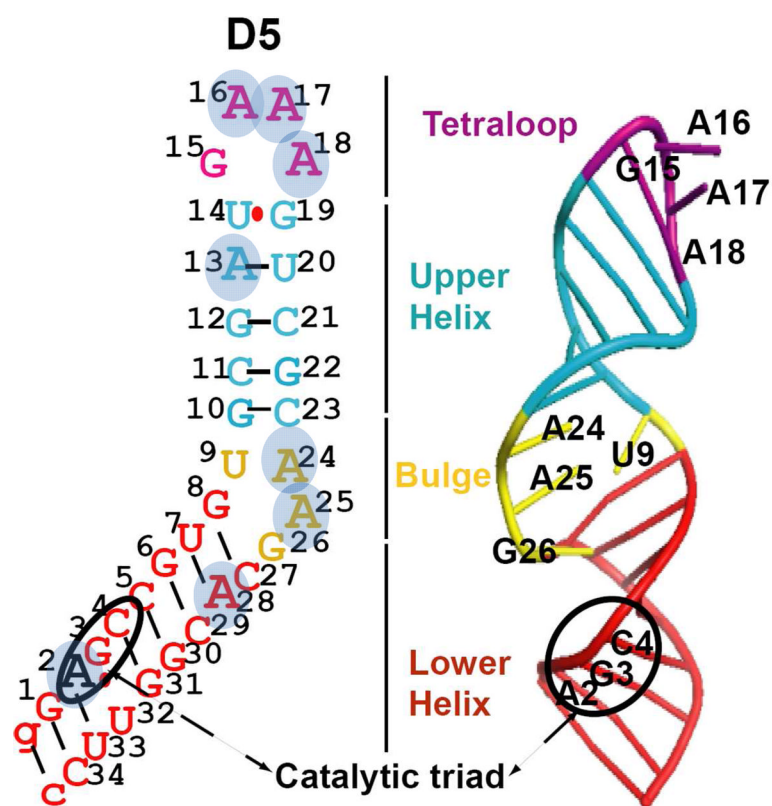


Figure 1. RNA secondary and solution NMR structure of D5-PL (21) (Protein Data Bank code 2F88) highlighting the tetraloop, catalytic triad, and internal bulge regions and all adenines labeled with ^{15}N and ^{13}C .

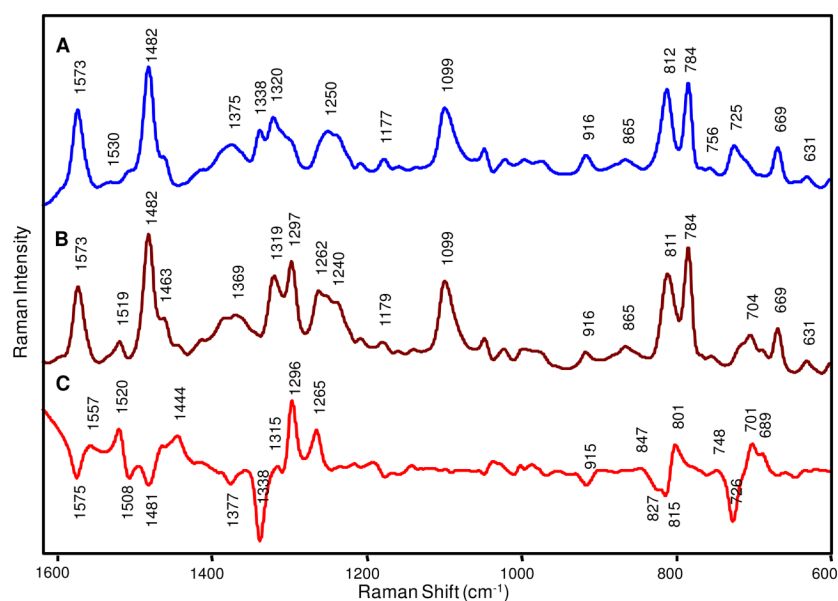


Figure 2.

Complete Raman spectra of 2 mM D5-PL in a 5 μ l hanging drop. A, Raman spectrum of unlabeled D5 RNA; B, Raman spectrum of D5-A-labeled RNA; C, Raman difference spectrum of D5-A-labeled minus unlabeled D5.

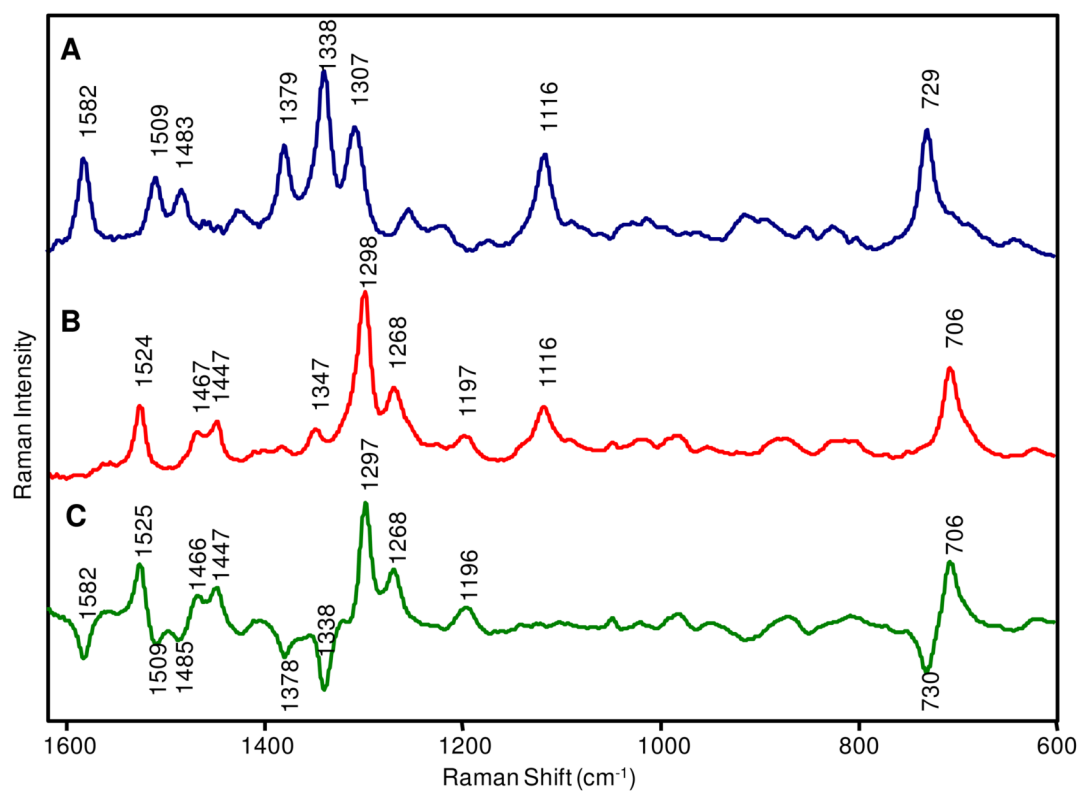


Figure 3. Solution Raman spectra of 10 mM ATP in a 5 μ l hanging drop. A, Unlabeled ATP; B, ^{15}N , ^{13}C labeled ATP; C, Raman difference spectrum of ^{15}N , ^{13}C labeled ATP minus unlabeled ATP.

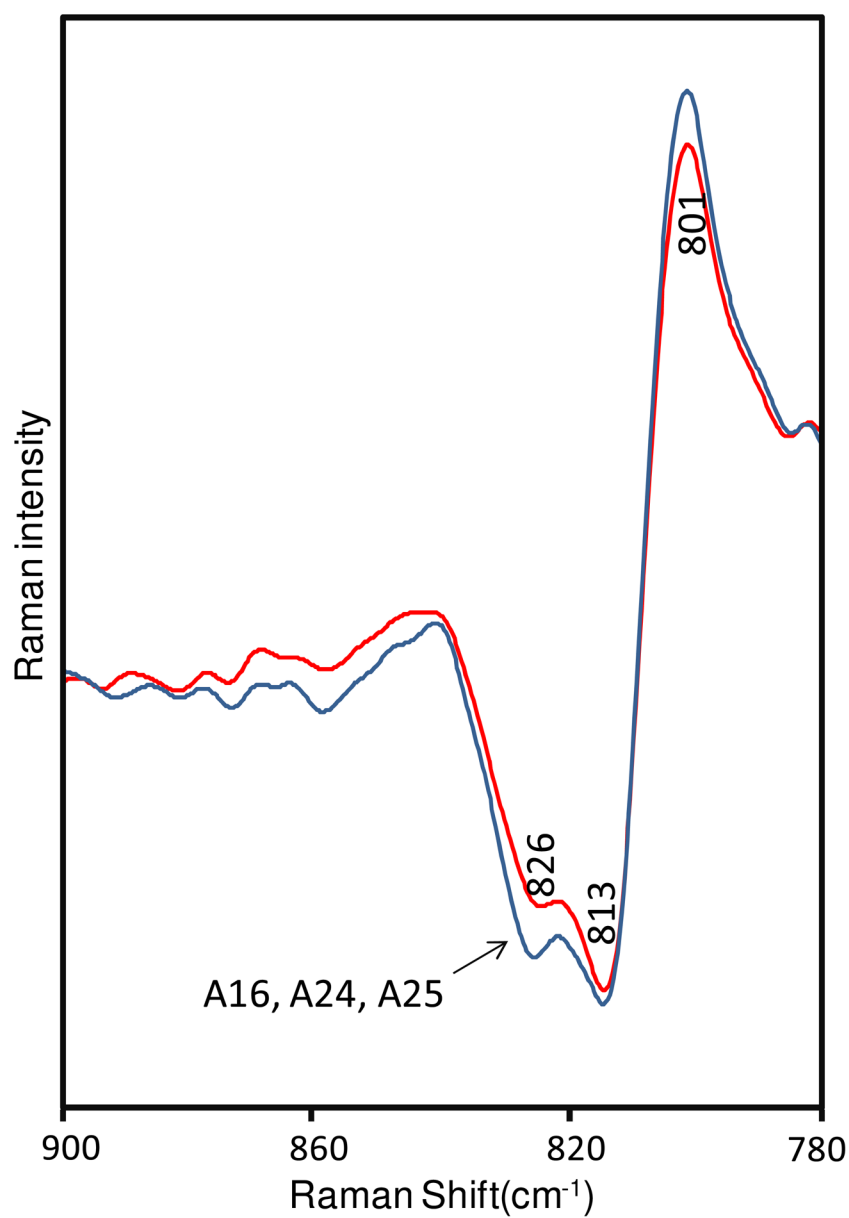


Figure 4. Partial Raman spectra of [A-labeled D5 without Mg²⁺] minus [unlabeled D5 without Mg²⁺] (red line) and [A-labeled D5 with 10 mM Mg²⁺] minus [unlabeled D5 with 10 mM Mg²⁺] (blue line).

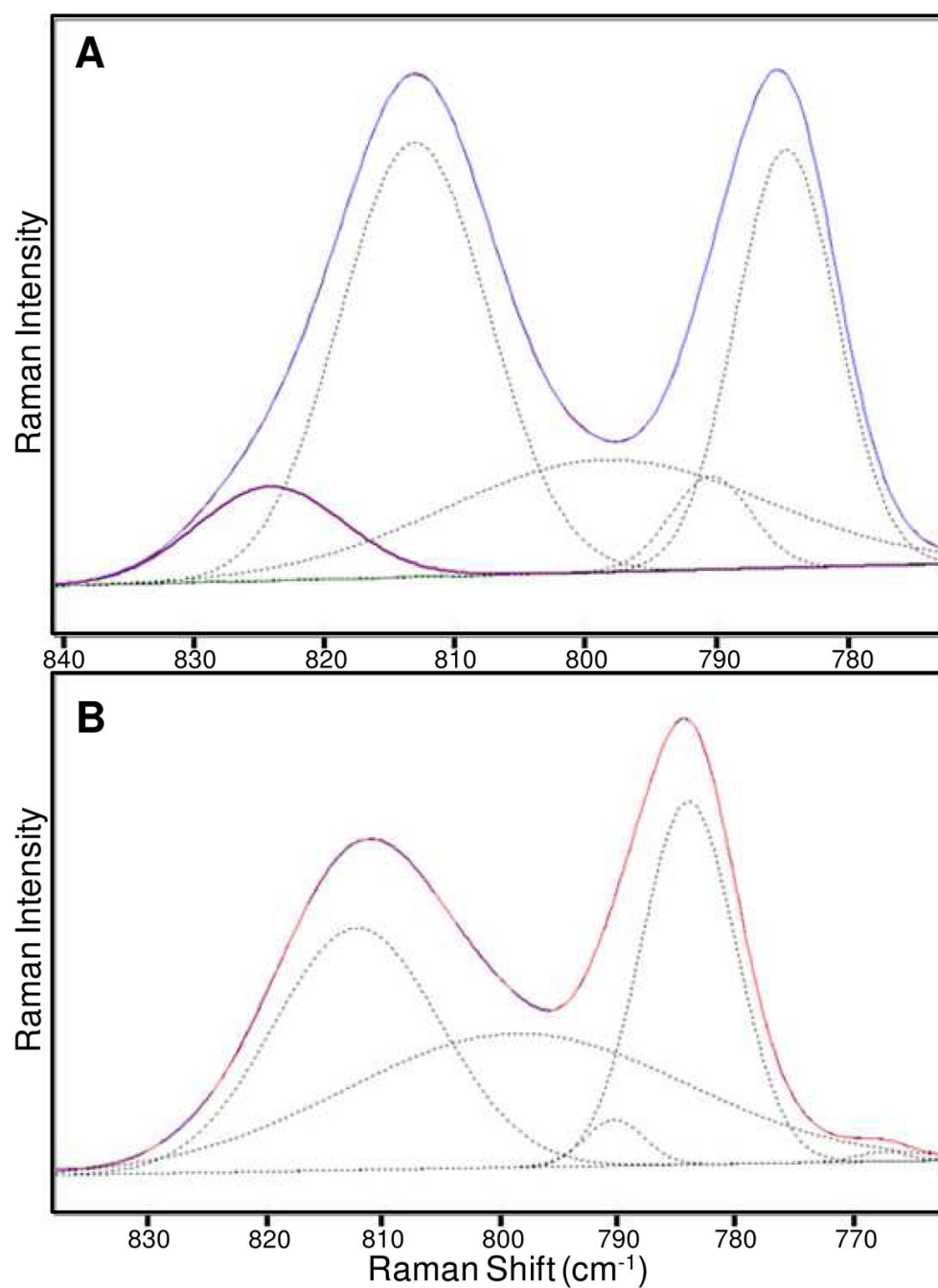


Figure 5. Peak fitting profiles for Raman spectra of (A) [unlabeled D5 without Mg²⁺] and (B) [A-labeled D5 without Mg²⁺]. Solid red and blue lines overlapping are Raman spectroscopic features and curve fitting results, separately. Dotted black lines are individual Gaussian peaks. The component at 824 cm⁻¹ is shown in purple.

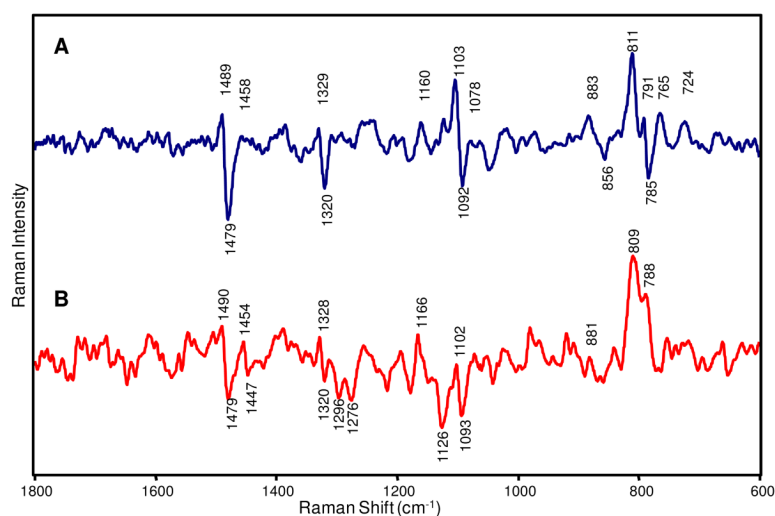


Figure 6. Raman difference spectrum of (A) [unlabeled D5 with 25 mM Mg²⁺] minus [unlabeled D5 without Mg²⁺] and (B) [A-labeled D5 with 10 mM Mg²⁺] minus [A-labeled D5 without Mg²⁺]

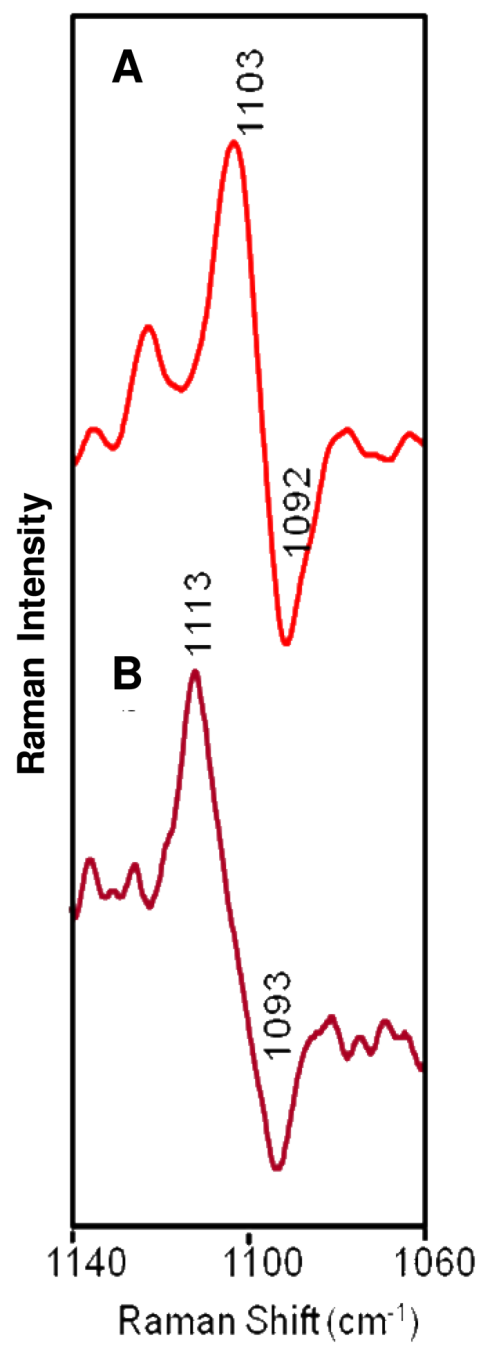


Figure 7. Raman difference spectra of (A) unlabeled D5 with 25 mM Mg²⁺ in the presence of 100 mM KCl and (B) unlabeled D5 with 25 mM Mg²⁺ in the presence of 100 mM NaCl.

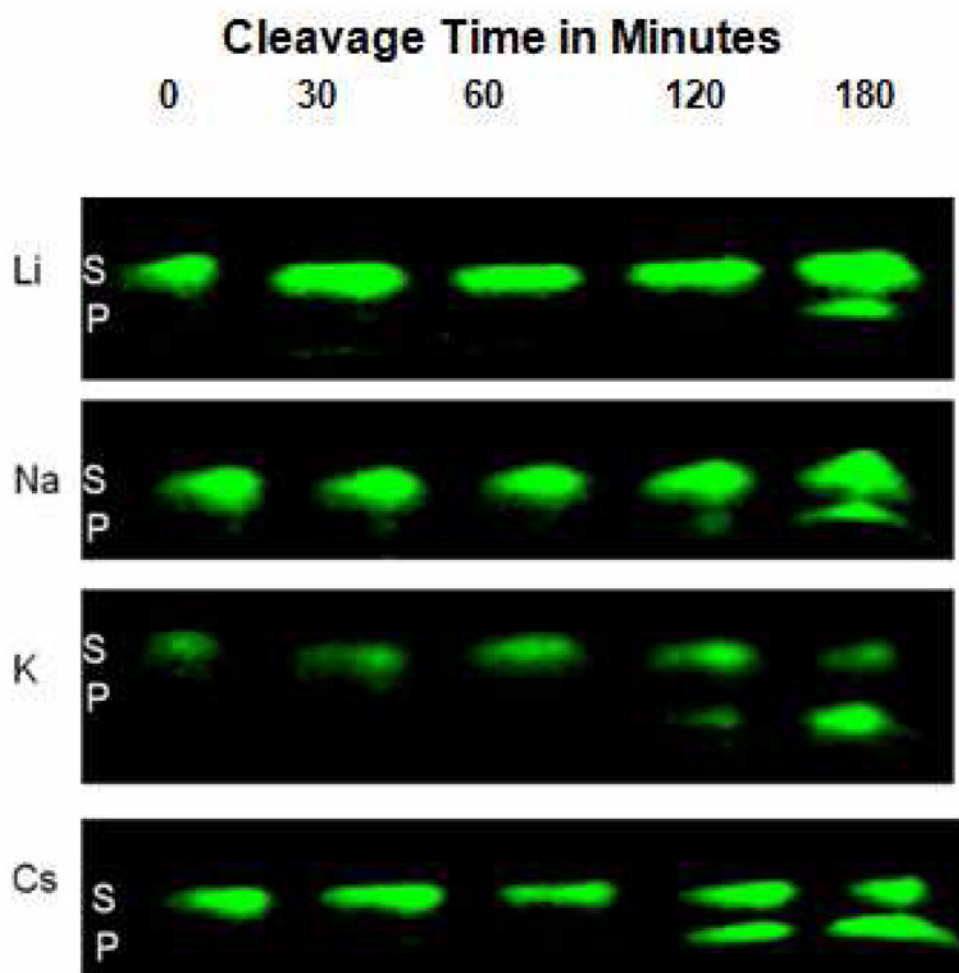


Figure 8.

Efficiency of trans-splicing (in the SER reaction) as a function of monovalent ion of 100 mM XCl, where X = Li⁺, Na⁺, K⁺, and Cs⁺ in the presence of 10 mM Mg²⁺. A time course of the SER cleavage reaction at pH 7.5. The fluorescence intensity in bands S (substrate) and P (cleaved product) was used to calculate the fraction of cleaved product.

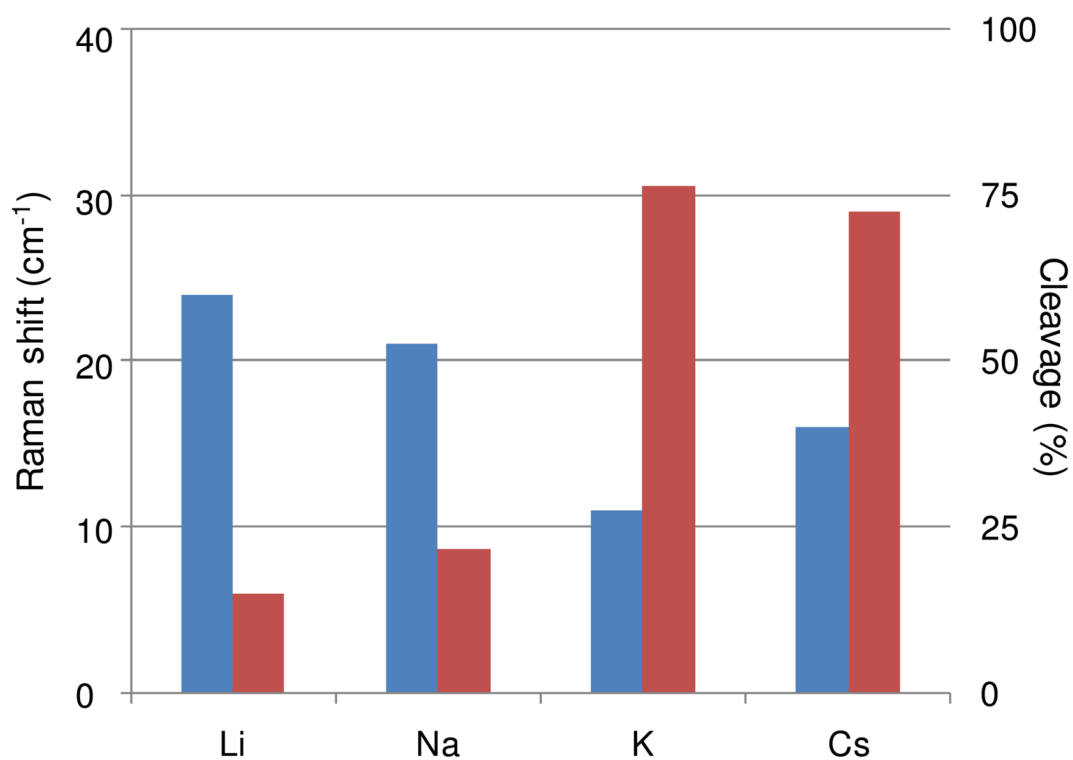


Figure 9.

Variation in efficiency of Raman shift and trans-splicing (in the SER reaction) as a function of monovalent ion of 100 mM XCl, where X = Li⁺, Na⁺, K⁺, and Cs⁺ in the presence of 10 mM Mg²⁺. The heights of blue bars equal Raman shift (cm⁻¹) of the PO₂⁻ mode in Raman difference spectra [D5 with Mg²⁺] minus [D5 with no Mg²⁺]; the heights of red bars equal fraction cleaved by the reconstructed D1235 RNA.

Table 1

Comparing the Raman features of unlabeled and ^{13}C , ^{15}N labeled adenosine (or ATP) calculated and experimental.

unlabeled (cm^{-1})		^{13}C ^{15}N labeled (cm^{-1})		Assignments
ATP (experimental)	Adenosine (calculated)	ATP (experimental)	Adenosine (calculated)	
730	737	706	717	A ring and ribose ring breathing
869	879	842	859	ribose breathing
1116	-	1117	-	non-bridging phosphate (49)
1253	1228	1196	1208	A ring mode and ribose CH, OH bending
1307	1272	1268	1240	A ring mode and ribose CH, OH bending
1339	1322	1298	1291	A ring mode and ribose CH, OH bending
1379	1371	1347	1326	A ring mode and ribose CH, OH bending
1426	1400	1382	1366	A ring mode
1459	1446	1404	1405	A ring mode
1483	1504	1447	1466	A ring mode
1510	1526	1467	1481	A ring mode
1582	1608	1524	1549	A ring mode

Table 2

The Raman upshift of PO_2^- band due to Mg^{2+} binding (at 10 mM) is affected by monovalent ion background (100 mM) of D5 samples.

Ion	Ionic Radii (58) (\AA)	$d_{\text{ion-W}}$ (59,60) (\AA)	Raman Upshift of PO_2^- Band Due to Mg^{2+} binding (cm^{-1})
Li^+	0.71	1.92–2.28	24 ± 3
Na^+	0.97	2.31–2.50	21 ± 2
K^+	1.41	2.60–2.92	11 ± 1
Cs^+	1.73	2.95–3.21	16 ± 3

$d_{\text{ion-W}}$ is the distance between the center of ion and the center of oxygen in H_2O